CICE2023 Rio de Janeiro - Brazil 11TH INTERNATIONAL CONFERENCE ON FRP COMPOSITES IN CIVIL ENGINEERING

FATIGUE PERFOMANCE OF INJECTED STEEL REINFORCED RESIN CONNECTORS IN GFRP SANDWICH WEB CORE PANELS

Angeliki Christoforidou, Delft University of Technlogy, The Netherlands, a.christoforidou@tudelft.nl
Martijn Veltkamp, FiberCore Europe, The Netherlands, veltkamp@fibercore-europe.com
Fruzsina Csillag; Arup Infrastructure, The Netherlands, Fruzsina.Csillag@arup.com
Liesbeth Tromp; Royal HaskoningDHV Infrastructure, The Netherlands, liesbeth.tromp@rhdhv.com
Marko Pavlovic; Delft University of Technlogy, The Netherlands, m.pavlovic@tudelft.nl

ABSTRACT
While Glass Fibre-Reinforced Polymer (GFRP) decks offer a competitive solution for bridge construction and renovation, their application is constrained by the absence of feasible, fatigue-resistant connection technologies. Current methods, including bolted, bonded, and cementitious grout-based connections, exhibit various limitations. The emerging injected Steel Reinforced Resin (iSRR) connector technology promises enhanced performance. However, its behaviour within a realistic bridge deck scenario, particularly under the influence of web direction, remains under-explored. This paper scrutinises these connectors in a sandwich web core panel setup, subjected to fully reversed loading cycles and post-fatigue static tests, with the aid of Finite Element modelling.

KEYWORDS
Injected Steel Reinforced Resin (iSRR) connector; bolted connection; sandwich web-core panel; fatigue; shear resistance

INTRODUCTION
In recent years, Fibre-Reinforced Polymer (FRP) sandwich foam core panels with or without interconnected webs, have revolutionized numerous high-performance applications due to their unique lightweight yet robust construction. Encapsulating a foam core between resilient outer and inner skins, these panels offer superior thermal and acoustic insulation properties, proving advantageous across various sectors. Their versatile use extends from serving as effective materials in residential to industrial construction (Shawkat et al., 2008), to enabling lightweight design in the aerospace (Castanié et al., 2020) and automotive sectors, and even enhancing the resilience of wind turbine blades in the renewable energy industry.

Building on their broad applications, in mid 1990s the use of Glass FRP (GFRP) sandwich foam core panels has permeated the field of bridge construction and renovation as described by (Zureick et al., 1995) and (Keller, 2003). However, the lack of a universally accepted, efficient, and predictable connection technology represents a significant barrier to the broader application of GFRP decks in the infrastructure sector. Recognizing the necessity for robust connection methodologies, industry and academia have investigated and developed bolted and bonded solutions to integrate GFRP panels in construction (Zetterberg et al., 2001; Zhou & Keller, 2005). Bolted connections, though simple and adjustable, can induce stress concentrations and compromise the integrity of the GFRP material. Bonded connections, while capable of distributing loads more evenly and maintaining the material's holistic integrity, can pose challenges with regard to long-term durability, inspection, and quality control.

A promising advancement in bridge construction technology is the introduction of the injected Steel-Reinforced Resin (iSRR) connector, designed for GFRP deck panels in hybrid steel-FRP bridges (Csillag, 2018). As shown in Figure 1, the iSRR connector, comprises double nuts (or a coupler) on a bolt/rod embedded within an FRP deck cavity, filled with steel shot particles and polymer resin. The iSRR connector leverages the enhanced properties of SRR injection material (Nijgh, 2017, 2021) to

form a resilient and fatigue-enduring connection by combining bolt preloading and injection, offering flexibility with options for prefabrication or on-site construction. Performance evaluations have demonstrated an impressive initial stiffness, shear resistance, and ultimate slip at failure, with fatigue endurance under fully reversed cyclic loading about 100 times greater than traditional bolted connections (Csillag & Pavlović, 2021; Olivier et al., 2021). However, especially the fatigue perfomance evaluations were based on laminate level tests and did not incorporate the connector within a GFRP deck panel.

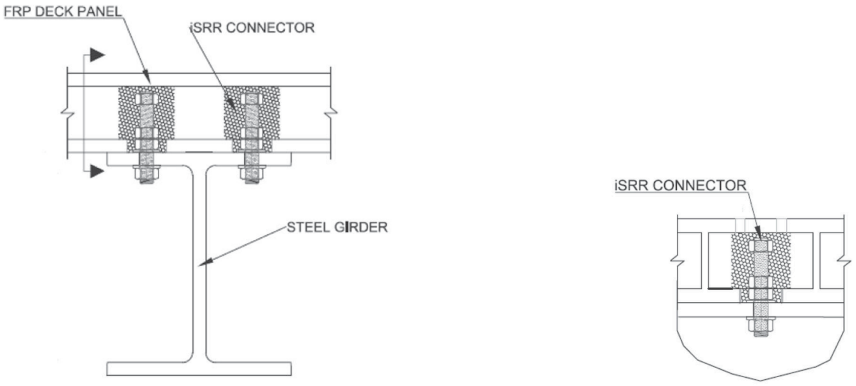

(a) Transverese direction of the beam (b) Longitudinal direction of the beam

Figure 1: iSRR connector embedded in a GFRP sandwich panel connected to steel girder. Photos taken from (Olivier et al., 2023)

Consequently, this study aims to examine the fatigue endurance and post-fatigue static performance of iSRR connectors embedded in a GFRP sandwich web core panel. A single lap joint (SLJ) setup, proven representative for characterising iSRR connector fatigue life (Olivier et al., 2023), is adopted and steel stiffeners are strategically employed in the steel plates to mitigate excessive flexibility in comparison to individual iSRR connector setups. The connectors will be subjected to fully reversed loading cycles with a maximum shear load of 60kN, subsequent to which post-fatigue static tests will be conducted. Since the connectors usually encounter shear loading in both directions, the impact of the web direction, along with the associated effect of the fiber direction of the bottom facing, is thoroughly examined. Finite Element (FE) models will be constructed to deepen our understanding of the webs' role in load transfer behavior, fatigue, and post-fatigue static performance of the iSRR connectors, potentially enhancing their practical application in bridge construction.

EXPERIMENTAL APPROACH

Specimens materials and dimensions

The GFRP deck panel, featuring interconnected webs, is produced through a vacuum infusion process. The followed procedure employs 5 Z-layers, providing fiber continuity between the facings and the webs, as discussed in (De Corte et al., 2017). The materials used include uni-directional fabrics of 1200 g/m^2 and 600 g/m^2 ±45° E-glass fibre reinforcement, which are embedded in a polyester resin. The outcome is a multidirectional, anisotropic laminate in the facings (0°/56.7%; 90°/16.7%; ±45°/26.6%) and a (0°/11.1%; 90°/11.1%; ±45°/77.8%) laminate in the webs with fibre volume fraction of Vf = 56% and Vf = 27%, respectively. These production details yield 20 mm thick skins and webs with 10 mm thickness, which are equally spaced every 150 mm. The total height of the panel is equal to 300 mm and 600x300 mm segments are cut from the complete panel. The orientation of the principal fiber direction is parallel to the loading direction.

The composition of the iSRR connectors is detailed as follows: they incorporate grade 10.9 M27 bolts, accompanied by three embedded nuts, and feature a semi-embedded washer, as delineated in the referenced literature (Christoforidou & Pavlović, 2023). The SRR material fills an 80 mm diameter circular hole in the bottom facing, an internal cavity measuring 100 mm in diameter by 150 mm in height, and a ridge area interfacing between the FRP deck and the steel end detail. The latter inclusion of SRR serves to manage the injection process and accommodate the irregularity of the bottom facing.

Test methodology and instrumentation

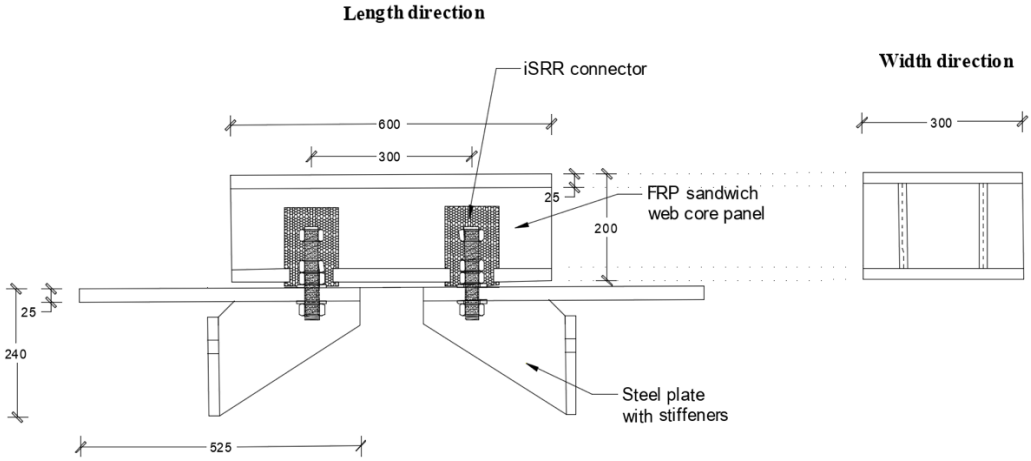

(a) Webs of GFRP panel parallel to the loading direction – W0

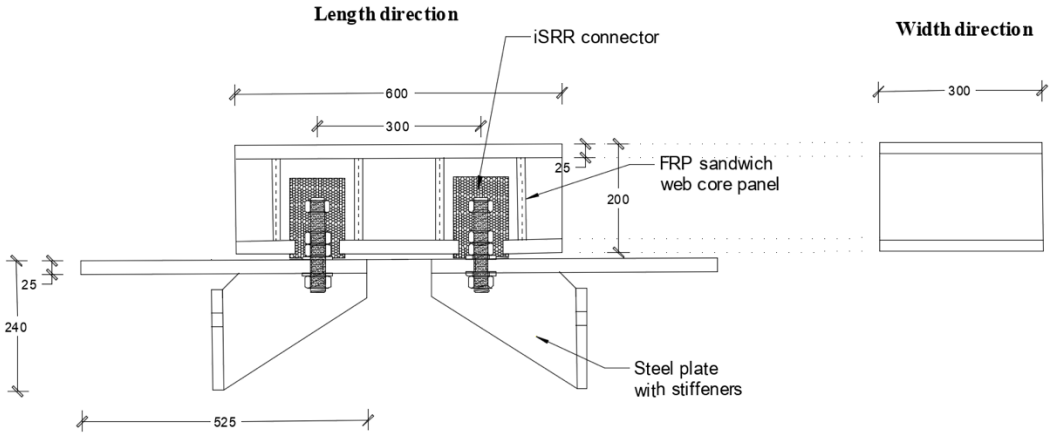

(b) Webs of GFRP panel perpendicular to the loading direction – W90

Figure 2: Dimensions of the test configuration

Both the static and the fatigue experiments are performed on an Instron 600 kN machine and are conducted under ambient laboratory conditions. The testing apparatus records the load-stroke responses and the number of cycles. To measure the variation in relative joint displacements between the FRP and steel plate, four Linear Variable Displacement Transducers (LVDTs) are mounted. Each connector employs two LVDTs, with the mean of these two values representing the relative joint displacement. These LVDTs are strategically positioned, one on the right and the other on the left of each of the connectors.

Figure 3: Test set up – Specimen with webs perpendicular to shear loading direction denoted as W90

For the cyclic experiments, the specimens undergo sinusoidal loading waveforms with a constant amplitude of 60 kN and a load ratio of -1 ($R=F_{min}/F_{max}$). A 4 Hz frequency is selected based on its established detrimental impact on injected bolts (van Wingerde et al., 2013), thus providing a valid basis for characterising the fatigue behaviour of iSRR connectors and a reasonable time frame to perform all tests. For the post-fatigue static tests a tensile monotonic loading is applied under a displacement control of 0.01 mm/s. No study is conducted on the effect of the loading rate.

While monitoring the increase in the displacement range of the connectors is essential, it is deemed impracticable to conduct the test until the often-cited 0.3 mm failure criterion in the literature is met (EN, 2008; Olivier et al., 2021). To facilitate a comparison among specimens with webs of the GFRP panel oriented in different directions, a specific cycle count has been established as the test termination point. Specifically, the test concludes after 5 days i.e., 1.7 million at ±60 kN.

Each specimen is identified by several factors: the prefix "F" or "PFS" denotes fatigue or post-fatigue static loading, respectively. Subsequently, the next designator represents the orientation of the webs. Specifically, we utilize the naming convention "W0" when webs are oriented parallel to the loading direction, and "W90" when they are perpendicular. The final element in the identification sequence signifies the numerical order of the connector tested within the same configuration and specimen. For each specimen, two connectors are tested, designated as top (number 1 or 3) and bottom (number 2 or 4) connectors.

Results from experimental campaign

Fatigue behaviour

Figure 4 presents the growth of relative slip against the number of cycles at various load levels. Given the absence of observable failure, the typical three-stage behaviour often associated with cyclic experiments involving FRP materials does not manifest. However, upon rendering the results in a double logarithmic scale, the onset of a second stage becomes discernible. This observation could facilitate the extrapolation of the slope up to the 0.3 mm displacement threshold. Table 1 presents the observed slip increase at the manual termination of the experiment.

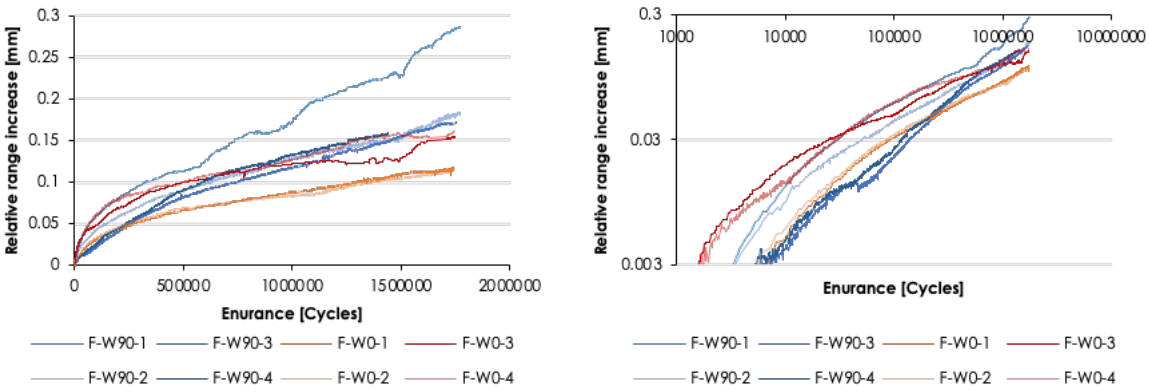

(a) Normal axis (b) Double logarithic axis

Figure 4: Relative slip increase versus number at different load levels

Table 1: Overview of fatigue experiments and results

Specimen designation	Observed slip increase (mm)
F-W90-1	0.284
F-W90-2	0.180
F-W90-3	0.171
F-W90-4	0.176

Average (COV):	0.203 (1.28%)
Specimen designation	**Observed slip increase (mm)**
F-W0-1	0.117
F-W0-2	0.113
F-W0-3	0.154
F-W0-4	0.160
Average (COV):	0.136 (8.25%)

Post-cyclic static behaviour

Figure 5 presents the representative load versus relative displacement responses for the iSRR connectors subjected to post-fatigue monotonic loading. The elastic stiffness acquired for each connector, in conjunction with their peak resistance, is outlined in Table 2. When the webs are oriented parallel to the direction of the shear load, the observed stiffness of the connection averages around 230.86 kN/mm. Interestingly, this value is notably reduced when the webs are oriented perpendicularly to the shear load, with the connector stiffness dropping to an average of 174.67 kN/mm. This signifies a decrease of roughly 24.4%, which emphasizes the importance of web orientation on the structural performance of the connectors within the system.

The final condition of the specimens, following the completion of the loading protocol, is illustrated in Figure 6. Visible cracks appear in the SRR piece, located outside of the FRP deck, along with evident debonding between the SRR piece and the internal nuts. The test halts manually once a load plateau is reached, which precludes attaining maximum possible ductility and eventual bolt fracture. However, subsequent testing as presented in (Christoforidou & Pavlović, 2023) corroborates that bolt fracture indeed governs the failure mechanism.

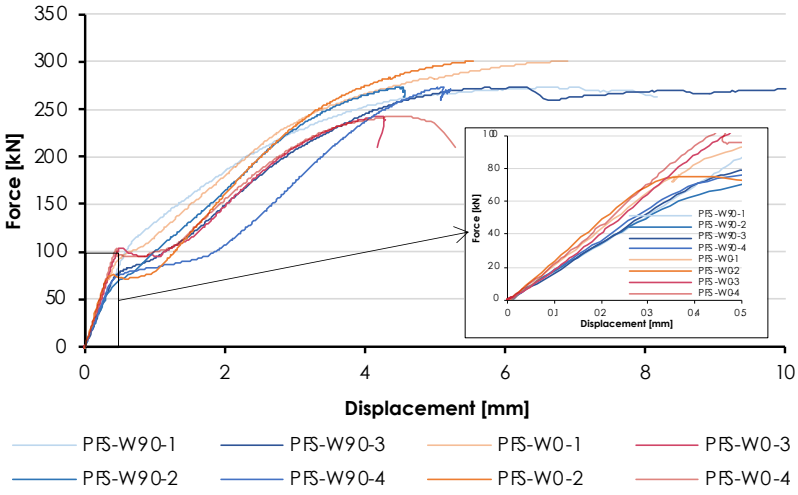

Figure 5: Post-fatigue static load-relative slip increase

Table 2: Overview of post-fatigue static experiments and results

Specimen designation	Elastic stiffness [kN/mm]	Resistance (kN)
PFS-W90-1	163.05	273.47
PFS-W90-2	171.66	
PFS-W90-3	180.92	273.51
PFS-W90-4	183.03	
Average:	174.7 (4.55%)	273.49 (0.01%)
PFS-W0-1	223.99	301.12
PFS-W0-2	247.10	
PFS-W0-3	218.81	243.11
PFS-W0-4	233.54	

Average:	230.86 (4.66%)	230.86 (10.66%)

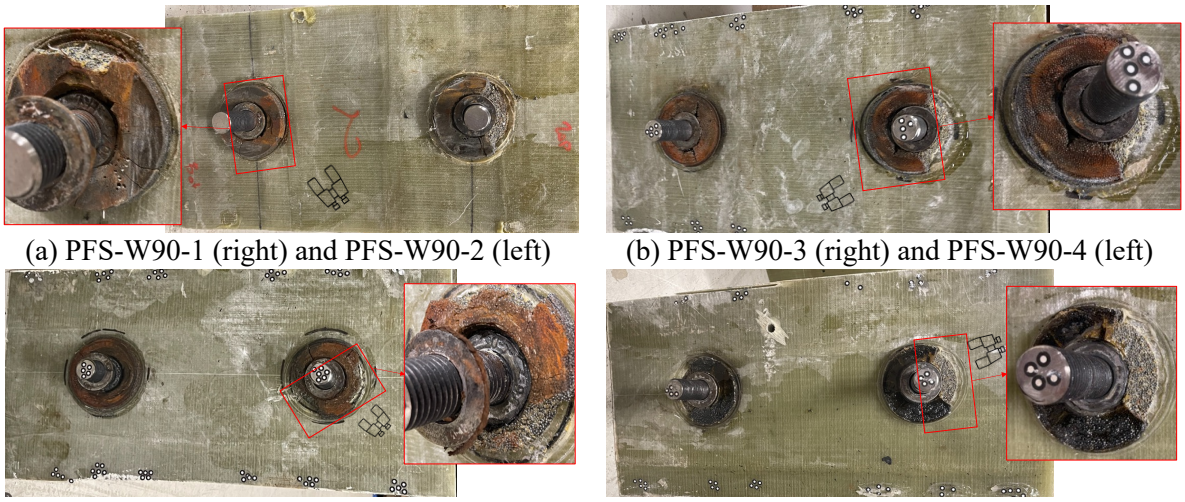

(a) PFS-W90-1 (right) and PFS-W90-2 (left) (b) PFS-W90-3 (right) and PFS-W90-4 (left)

(c) PFS-W0-1 (right) and PFS-W0-2 (left) (d) PFS-W0-3 (right) and PFS-W0-4 (left)

Figure 6: Cracks in SRR piece and debonding between SRR and nut after completion of static loading

Discussion

The outcomes of post-fatigue static loading tests highlight a discernible distinction between connectors embedded in webs orientated parallel or perpendicular to the loading direction. To elucidate whether this difference stems from the fiber direction at a local scale - where one of the LVDTs brackets is mounted, or from the variable slip increments aquired in the prior fatigue testing, Figure 7 has been constructed. This figure establishes a correlation between the relative displacement range increase as measured by the LVDTs and the elastic stiffness derived from the post-fatigue cyclic tests.

The observed correlation distinctly signifies an interdependence between the two variables, suggesting that the initial cyclic loading preceding the monotonic tests directly influences the elastic stiffness of the connector, a phenomenon also observed in the work of (Liu et al., 2021). To best represent this relationship, three distinct fitting functions were applied: a second-order polynomial, a linear function, and a power law function. Each model was evaluated based on its goodness of fit, as indicated by the R^2 value. Among the tested models, the second-order polynomial fitting function demonstrated the highest R^2 value, thereby providing the most precise representation of the existing relationship between the two parameters. Even though the polynomial function provides the best fit, the modest R^2 value suggests that additional data collection may be necessary for enhanced model accuracy.

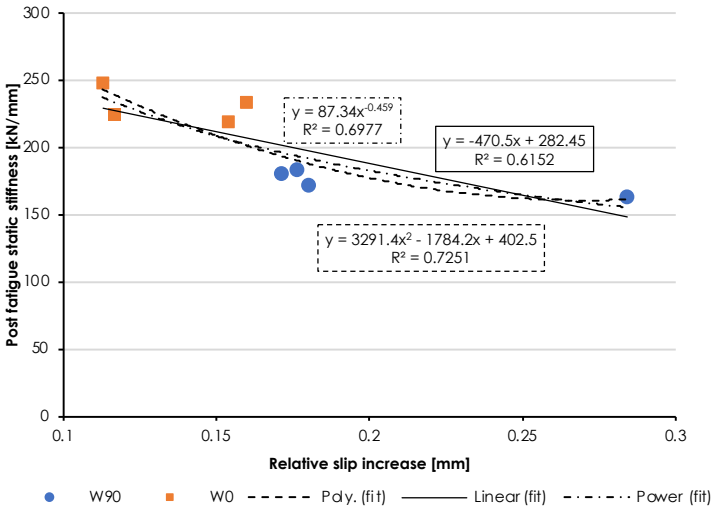

Figure 7: Post-fatigue static stiffness versus relative slip increase

NUMERICAL ANALYSIS

Description of the model

The FE models are composed of half of the GFRP deck with the embdedded iSRR bolted connector and one steel end detail that includes a steel plate with the two stiffeners. The iSRR connection is explicitely modelled with the embedded bolts, nuts and washer excluding the threaded parts.Since the threads were omitted, the rods were not modelled utilising their major or pitch diameter but instead their minor diameter of 23 mm is inputted. This would result in a representative damage model of an M27 bolt as provided in (Pavlović, 2013).

Simulating the single lap test requires defining symmetry boundary conditions on the end surface of the GFRP deck segment, as depicted in Figure 8. Two steps are performed in the analysis, with the first one corresponding to the preloading of the bolts and the second one with the application of the loading. To start, the bolts are preloaded by thermally contracting the bolt rod using the predefined field option as in (Egan et al., 2012; Liu et al., 2019). Then, the load is applied as a prescribed displacement on three reference points in the steel end detail kinematically coupled to their corresponding surfaces. Both steps are assigned with a smooth amplitude curve to prevent creation of inertia forces.

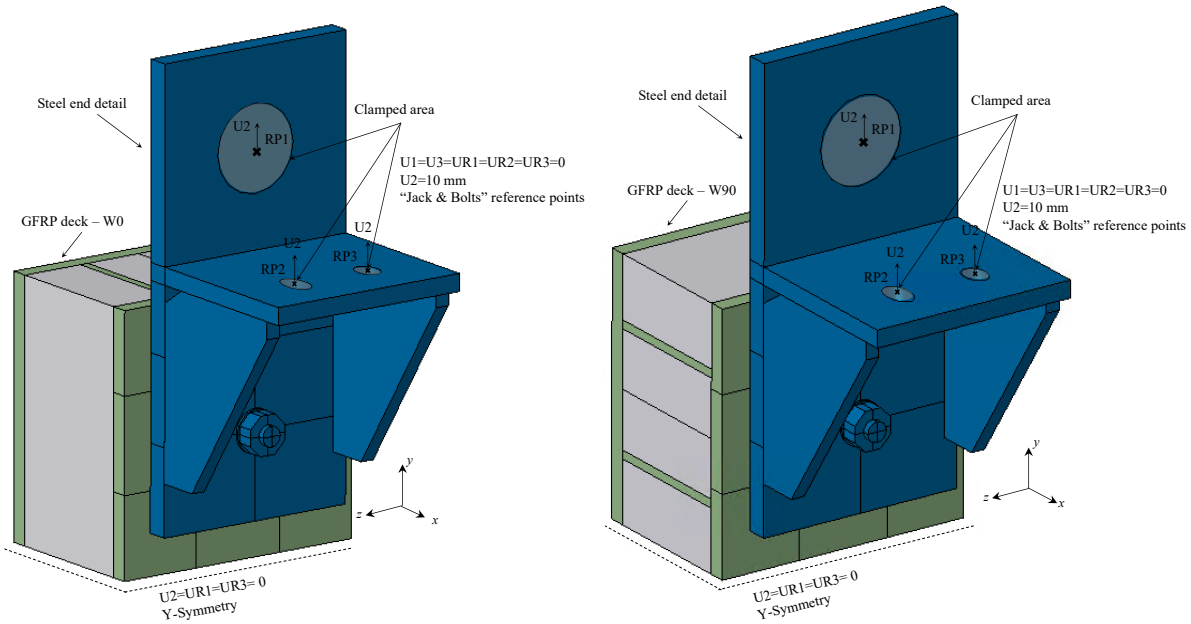

(a) Webs parallel to the loading direction – W0 (b) Webs parallel to the loading direction – W90
Figure 8: Assembly and boundary conditions of the FE models

Materials and mesh

The steel parts are modelled as linear elastic (E=210 GPa and v=0.3), isotropic and no fracture was defined. On the other hand, due to bolt failure in the experiments, the bolts' material property includes ductile and shear damage as defined in (Pavlović, 2013) for 10.9 bolts. To achieve the desired prestress in the bolt by appling a predefiened field, the bolt rod is described as an orthotropic material with thermal expansion properties.

Concrete Damage Plasticity (CDP) model is used for the representation of steel reinforced resin. The elastic constants and tensile strength of the SRR are obtained from (Christoforidou et al., 2023) where tensile splitting tests and FE analyses were conducted. More specifically, the Young's modulus and tension strength are E = 16.2 GPa and f_t = 10.1 MPa, respectively and the Poisson ratio is numerically obtained as ν = 0.13. For the compression strength, a mean value of f_c = 180 MPa which corresponds to the values reported by (Nijgh, 2021) for confined SRR material.

Table 3: Material properties

Material	Elastic constants [MPa]	Poisson's ratio	Nonlinear material model
Steel (except bolt)	E=210000	*v*=0.3	-
Bolt	E=210000	*v*=0.3	Damage model of 10.9 bolts from (Pavlović, 2013)
GFRP UD ply facings	E_1=31450, E_2=E_3=8459, G_{12}= G_{13}=4838, G_{23}=3021	ν_{12}= ν_{13}=0.28, ν_{23}=0.4	Hashin damage model from (Csillag, 2018)
GFRP UD ply webs	E_1=21170, E_2=E_3=5690, G_{12}= G_{13}=3260, G_{23}=2032	ν_{12}= ν_{13}=0.28, ν_{23}=0.4	-
SRR	E=16181	ν=0.13	Concrete damage plasticity model based on (Christoforidou et al., 2023)
Foam	E=2.1	ν=0.2	Stress strain curve from (Tuwair et al., 2015)

The assembly comprising the bolt, four nuts, two washers, and the SRR utilizes linear, four-noded C3D4 tetrahedron elements to replicate their geometry. The steel end detail consists of a steel plate and stiffeners made out of linear, eight-noded solid C3D8R elements with reduced integration and enhanced hourglass control. The GFRP composite plate employs the 2.5D stacked-shell approach. The laminate is partitioned into five sub-laminates along the thickness, composed of eight-noded SC8R quadrilateral in-plane general-purpose continuum shell elements. A global mesh size of 5 mm is used in the models, with a denser mesh around the shear connectors: the bolt employed a 1.2 mm element size in between the two washers, while the GFRP facing encircling the hole used 1 mm tangential and radial mesh in the continuum shell elements (Figure 9).

a) Steel end detail b) GFRP deck + sublaminates c) iSRR connector

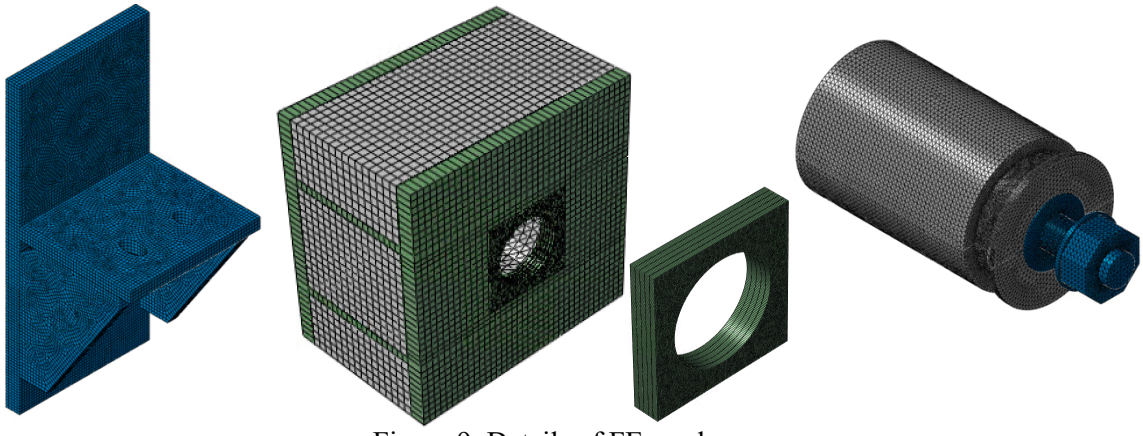

Figure 9: Details of FE mesh

Interaction properties

The actual stacking sequence of the FRP skins and webs is assigned and sublaminates are defined at the regions where delaminations could be expected. The transversely isotropic elastic material properties of the UD plies constituting the facings and the webs are given in Table 4. In between the sublaminates, cohesive surface interaction property is applied to account for delamination damage. The interface strength and fracture energy values of the CZM model are given in Table X and are calibrated from compressive loading models on the same GFRP deck segments. The foam of the GFRP deck is modelled utilising the compressive test results for low-density foams reported in in (Tuwair et al., 2015).

Table 4: Cohesive surface interaction properties in between sublaminates

	Normal mode I	**Shear mode II**	**Shear mode III**
Contact strength [MPa]	21	30	30
Fracture energy [N/mm]	0.9	4	4

The definition of the interaction between the SRR material and the bolt, nuts, washer, and FRP facing is critical, but there is no indication of what it should be. Given the assumption that after the completion of the fatigue test, the SRR material might exhibit cracks or debonding from its interconnected surfaces, two models are constructed per each geometry (webs in 0 and webs in 90 direction). The first, referred to as 'Tie', assumes an undamaged SRR block and interfaces, while the second, 'Friction', assumes a friction coefficient of 0.2 within the SRR material and between all its contacting components (e.g., GFRP bottom facing, foam, bolt rod, nuts, and washer), representing potential internal and external cracks. A friction coefficient of 0.2 is also introduced between the washers and steel plate, chosen to closely replicate actual slip conditions.

Results

The force-displacement curves up until the slip resistance are derived from FE modelling (Figure 10 (a)) and they demonstrate negligible variations in the system's static performance as a result of alternating the orientation of the webs and, correspondingly, the principal fiber direction. The observable differences in performance can be predominantly attributed to the varied interaction properties associated with the SRR component as it can be seen in Figure 10 (b). In situations where the SRR block is subjected to tied constraints, thus preventing the occurrence of cracks, the system exhibits an enhanced initial stiffness. Conversely, when friction is introduced, the system displays a more compliant response, leading to increased overall ductility. Particularly for the orientation of fibers (and webs) perpendicular to the loading direction, a friction coefficient of 0.2 appears to effectively capture the lower bound of the connectors' stiffness.

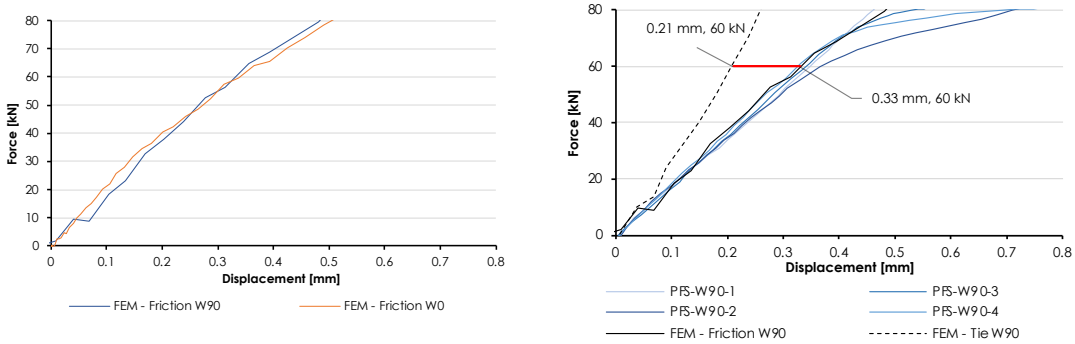

(a) Different web direction (b) Experiments with W90 and FE prediction

Figure 10: Comparative force-displacement responses of iSRR Connector

In the preliminary stages of cyclic testing, it is reasonable to postulate that the SRR piece is bonded to the surfaces it contacts, akin to a tie constraint. Numerical results show that at a load of 60 kN, a relative slip of 0.21 mm can be expected. As the testing cycles proceed, debonding or cracks may initiate in the SRR piece. Assuming full cracks are developed, friction likely comes into play, yielding a relative slip of 0.33 mm at a load of 60 kN. Consequently, a slip increase of 0.12 mm from the start to the end of the cycles can be ascribed solely to cracks resulting from tension load. Given a load ratio of -1, a similar slip increase can be anticipated for the compression load of -60 kN. Hence, a total slip of 0.24 mm should be the maximum slip accumulation attributable to these failure mechanisms. This value should be higher than the experimentally derived values presented in Table 1 if no other effect is pronounced. Further analyses are warranted to comprehend the less pronounced slip range increase observed experimentally when the webs were oriented parallel to the loading direction.

CONCLUSIONS

This study was dedicated to investigating the fatigue endurance and post-fatigue static behavior of a novel type of slip resistant connectors integrated into a GFRP sandwich web core panel. The experimental investigation was performed under fatigue and post-fatigue SLJ tests. The iSRR connectors were subjected to full reversal loading cycles with an alternating shear load of ±60 kN, followed by post-fatigue static tests and the impact of the web direction was thoroughly examined. The numerical work assisted in expanding the understanding of how the web direction influences the load transfer behavior, fatigue life, and post-fatigue static performance of iSRR connectors. Drawing upon the extensive analysis and insights gained throughout this research, it can be summarized that:

1) It is adviced to test the fatigue performance of iSRR bolted connections embedded in an FRP deck with the webs oriented perpendicular to the shear loading direction for more adverse cyclic degradation based on their increased displacement range accumulation.
2) The post-fatigue static tests initially suggested a direct influence of web alignment in relation to the shear load direction on the connector's performance, as evidenced by a 24% decrease in stiffness when the webs were oriented perpendicular to the load direction. However, subsequent analysis clarified that the stiffness difference is primarily attributable to the prior cyclic testing, which resulted in less damage (in terms of relative slip increase) in that particular geometry.
3) The presented numerical work facilitates upper and lower bound estimations of the initial and fully degraded stiffness of the connectors, achieved by incorporating tie constraints or by introducing friction interaction within the SRR material and its interconnected elements, respectively. The friction-inclusive model aligns favorably with the lower bound observed in the post-fatigue static tests. The absolute difference in connector’s deformation between the lower and upper bound is 0.24 mm. If experimental observations show a greater slip at this load level, it is likely due to other failure mechanisms not captured in the current model. These additional mechanisms warrant further research for a complete understanding of their impact.

CITATIONS

Castanié, B., Bouvet, C., & Ginot, M. (2020). Review of composite sandwich structure in aeronautic applications. *Composites Part C: Open Access*, *1*, 100004.
Christoforidou, A., & Pavlović, M. (2023). Fatigue performance of FRP-steel connectors at room and elevated temperatures. *Submitted for publication*.
Christoforidou, A., Verleg, R., & Pavlović, M. (2023). Static, fatigue and hygroscopic performance of steel-reinforced resins under various temperatures. *Submitted for publication*.
Csillag, F. (2018). *Demountable deck-to-girder connection of FRP-steel hybrid bridges* [Master Thesis, Delft Technical University].
Csillag, F., & Pavlović, M. (2021). Push-out behaviour of demountable injected vs. blind-bolted connectors in FRP decks. *Composite Structures*, *270*. https://doi.org/10.1016/j.compstruct.2021.114043
De Corte, W., Jansseune, A., Van Paepegem, W., & Peeters, J. (2017). Structural behaviour and robustness assessment of an InfraCore inside bridge deck specimen subjected to static and dynamic local loading. Proceedings of the 21st International Conference on Composite Materials, Xi'an,
Egan, B., McCarthy, C., McCarthy, M., Gray, P., & Frizzell, R. (2012). Modelling a single-bolt countersunk composite joint using implicit and explicit finite element analysis. *Computational Materials Science*, *64*, 203-208.
EN, C. (2008). 1090-2: execution of steel structures and aluminium structures–part 2: technical requirements for steel structures. *European Committee for Standardisation, Brussels*.
Keller, T. (2003). *Use of fibre reinforced polymers in bridge construction*.
Liu, L., Wang, X., Wu, Z., & Keller, T. (2021). Tension-tension fatigue behavior of ductile adhesively-bonded FRP joints. *Composite Structures*, *268*, 113925.
Liu, W., Yu, F., He, Z., & Qing, G. (2019). A progressive damage model introducing temperature field for bolted composite joint with preload. *Modelling and Simulation in Materials Science and Engineering*, *27*(6), 065011.
Nijgh, M. P. (2017). *New Materials for Injected Bolted Connections - A Feasibility Study for Demountable Connections* [Master Thesis, Delft University of Technology].
Nijgh, M. P. (2021). *A multi-scale approach towards reusable steel-concrete composite floor systems* [PhD Thesis, Delft University of Technology].
Olivier, G., Csillag, F., Christoforidou, A., Tromp, E., Veltkamp, M., & Pavlović, M. (2023). Feasibility of bolted connectors in hybrid FRP-steel structures. *Construction and Building Materials*, *383*(131100).
Olivier, G., Csillag, F., Tromp, E., & Pavlović, M. (2021). Conventional vs. reinforced resin injected connectors' behaviour in static, fatigue and creep experiments on slip-resistant steel-FRP joints. *Engineering Structures*, *236*. https://doi.org/10.1016/j.engstruct.2021.112089
Pavlović, M. (2013). *Resistance of bolted shear connectors in prefabricated steel-concrete composite decks* University of Belgrade].
Shawkat, W., Honickman, H., & Fam, A. (2008). Investigation of a novel composite cladding wall panel in flexure. *Journal of Composite Materials*, *42*(3), 315-330.
Tuwair, H., Hopkins, M., Volz, J., ElGawady, M. A., Mohamed, M., Chandrashekhara, K., & Birman, V. (2015). Evaluation of sandwich panels with various polyurethane foam-cores and ribs. *Composites Part B: Engineering*, *79*, 262-276.
van Wingerde, A. M., van Delft, D. R. V., & Knudsen, E. S. (2013). Fatigue behaviour of bolted connections in pultruded FRP profiles. *Plastics, Rubber and Composites*, *32*(2), 71-76. https://doi.org/10.1179/146580103225009103
Zetterberg, T., Åström, B. T., Bäcklund, J., & Burman, M. (2001). On design of joints between composite profiles for bridge deck applications. *Composite Structures*, *51*(1), 83-91.
Zhou, A., & Keller, T. (2005). Joining techniques for fiber reinforced polymer composite bridge deck systems. *Composite Structures*, *69*(3), 336-345.
Zureick, A.-H., Shih, B., & Munley, E. (1995). Fiber-reinforced polymeric bridge decks. *Structural Engineering Review*, *3*(7), 257-266.

ACKNOWLEDGEMENT

The authors gratefully acknowledge the generous financial support provided by RWS, which has been instrumental in the successful completion of this research, as well as FiberCore Europe and AOC Resins for kindly supplying the essential resources that greatly contributed to the advancement of our work.

CONFLICT OF INTEREST

The authors declare that they have no conflicts of interest associated with the work presented in this paper.

DATA AVAILABILITY

Data on which this paper is based is available from the authors upon reasonable request.